Nonlinear phase shifts induced by semiconductor optical amplifiers with control pulses at repetition frequencies in the 40−160-GHz range for use in ultrahigh-speed all-optical signal processing

Yoshiyasu Ueno, Shigeru Nakamura, and Kazuhito Tajima

Networking Laboratories, NEC Corporation, 34 Miyukigaoka, Tsukuba, Ibaraki 305-8501, Japan

In a semiconductor optical amplifier (SOA) with copropagating optical pump pulses, the application of a nonlinear phase shift to optical signals provides the driving force for all-optical interferometric switching. We study, both analytically and experimentally, the dependencies of the nonlinear phase shift on the driving frequency (42–168 GHz) and on the SOA parameters. We have found that the nonlinear phase shift ($\Delta\Phi_{\text{NL}}$) decreases with the driving frequency but that this decrease is only linear, i.e., $\Delta\Phi_{\text{NL}} \propto f^{-1}$. We have also found that the nonlinear phase shift in the SOA linearly increases with the injection current (I_{op}), i.e., $\Delta\Phi_{\text{NL}} \propto I_{\text{op}}$, even in this ultrahigh-frequency range. © 2002 Optical Society of America

OCIS codes: 060.0060, 120.5060, 190.5970, 190.7110, 320.7080, 320.7160.

1. INTRODUCTION

Ultrafast all-optical signal processors whose bandwidths possibly approach optical frequencies (e.g., 200 THz in optical communication) have fascinated optics researchers for more than three decades, i.e., since the birth of nonlinear optics.[1] The most basic unit of such a processor would be what is referred to as an all-optical switch. Thus far, however, the trade-off between the speed of switching and the power required for all-optical control, both of which are determined by the nonlinear optical properties applied to the switch, are perceived to have prevented the large-scale application of all-optical switches. When an all-optical switch is based on a nonlinear phenomenon that appears at some distance from its one-photon resonance, the switch requires a relatively strong optical control pulse or an extremely long interaction length; the latter approach is used in all-optical switches that are made from silica fibers. The typical control-pulse energy (peak power) for an all-optical AlGaAs waveguide switch operating in a band well below its one-photon resonance (slightly below its two-photon resonance) was 100 pJ (with a peak power of 200 W).[2] Such strong pulses are readily generated in laboratories but are not suitable for the optical communications industry. A switch may also be based on a nonlinearity in the vicinity of one-photon resonance of such a semiconductor waveguide, in which case the power required for all-optically controlling the switch is several orders of magnitude smaller. In this case it was generally assumed for some time that switching is necessarily slowed down by the relaxation time that is needed for the resonantly excited electrons in the material to return to the ground state.

Researchers began to challenge that assumption in the late 1980s and the early 1990s, as they found that the relaxation time does not necessarily limit the speed of switching. The limitation does not apply when the switch consists of an optical nonlinear material embedded in an interferometer in a certain way; the symmetric Mach–Zehnder (SMZ) all-optical switch[3,4] and the terahertz optical asymmetric demultiplexer[5] are two examples. In these structures, as we explain later in the text, the interference effectively masks the relaxation of the nonlinear material. The interference is between two split optical components, where one of the two components is given a finite delay time, Δt. This interference effectively forms a rectangularlike window for switching by the all-optical switch, and the rise and fall times of the window are determined by the width of the control pulse rather than by the relaxation time. The window's width is determined by the delay time, Δt. Both an ultrafast response and a nearly rectangular shape for the switching window are important in obtaining timing-jitter-tolerant signal processing for an optical communications system.

In fact, a record response time (the sum of rise and fall times) of 200 fs has been reported for a SMZ switch.[6] In this device, each 130-fs-long control pulse in an 82-MHz train was absorbed by InGaAsP waveguides inside the switch. The control pulses generated electron–hole pairs (carriers), i.e., induced nonlinear changes in the refractive index because of the band-filling effect, imparted nonlinear phase shifts to the copropagating input signal and switched the signal after the interference while masking the relaxation time. The carrier relaxation time of the semiconductor material (100–200 ps, 3 orders of magnitude longer than the measured response time) did not limit the speed of the switch's response. The control pulse required for the 200-fs switching had 3 pJ of energy and a peak power level of 23 W. Near-rectangular

switching windows have been reported.[4,7] The control pulses for a SMZ switch that contains semiconductor optical amplifiers (SOAs) as the nonlinear elements require even lower levels of power. This is so because a smaller number of control-pulse photons is enough to generate a specific change in the number of carriers, which in turn creates a specific nonlinear phase shift (e.g., a shift of π). Response times of 0.67–1.0 ps have been recorded for such devices, with control pulses in the range 82 MHz–10 GHz.[8,9] The near-rectangular quality of the switching windows in these devices has also been confirmed.[9] Taking advantage of these fast response times and switching windows, the present authors and some of their colleagues have also demonstrated error-free 16:1 demultiplexing from 168 to 10.5 Gbits/s.[10,11] Only 50–80 fJ of energy was required in the control pulse (the peak power level of which was 25–40 mW). Note that the frequency of repetition for switching in the demultiplexer was 10.5 GHz (not 168 GHz).

For flexible processing and logical gating of ultrafast optical-time-division multiplexing (OTDM) signals, the frequency of repetition for switching (repetition frequency) is as important as the response time. For example, all-optical wavelength conversion,[12,13] reamplifying, reshaping, and retiming regeneration,[14] and asynchronous packet gating[15] have recently been attracting attention as devices that will play key roles in the building of efficient and flexible OTDM packet networks. In each of these signal-processing functions the switch must operate at the repetition frequency of the OTDM signal (e.g., 160 GHz) and must be driven by digitally coded pulses. The repetition frequencies in early experiments were in the range 80 MHz–10 GHz. Several teams of scientists have reported operation of the switches at 40 GHz.[12,16–19] Research has recently entered the 80–160 GHz range; examples include logic gating at 100 GHz,[20] 3R regeneration of random signals at 84 GHz,[21–23] and wavelength conversion of random signals at 168 GHz[21,24,25] (in all of the research cited in these publications the all-optical switches used were of the SMZ type).

However, no reports to date of which we are aware have included an analysis or investigation of the dynamics of the nonlinear phase shift in SOAs driven at ultrahigh frequencies. Specifically, although the nonlinear phase shift is known to decrease with the driving frequency, nobody has reported studying the steepness of this decrease. Durhuus *et al.*[26] and Joergensen *et al.*[27] have analyzed the SOA's nonlinear response to sinusoidally modulated input lights as a function of repetition frequency. The approach of each team was similar to the small-signal analysis that is conventionally used to analyze the direct modulation of semiconductor lasers. The driving force for SMZ-type switching is, however, the impulselike nonlinear phase shift (jump) that is induced by short control pulses. Being able to obtain a phase shift of π is particularly important not only because this is necessary to ensure perfectly constructive interference in forming the switching window[3] but also because the sinusoidal transfer function of the interferometer inside the switch suppresses noise in the signal intensity at a phase shift of π.[28] Despite its importance, most previous high-repetition-rate experiments (with a few exceptions[16,29])

have not included measurement of the magnitude of the nonlinear phase shift. Part of the reason for this is the difficulty of measuring the magnitude of a nonlinear phase shift that coexists with strong gain modulation.

We report here our experimental study of the dynamics of the nonlinear phase shift applied by a SOA operating at repetition frequencies in the 42–168-GHz range. First, in Section 2 we introduce several all-optical semiconductor switches of the SMZ type. In Section 3 we introduce a theoretical background to the nonlinear dynamics and a form of numerical simulation that we recently developed. After describing our verification of the correspondence between the results of simulation and experiment in the 10–40-GHz range, we discuss the use of the simulation to investigate the dependencies of the nonlinear phase shift on many important SOA parameters. We also describe a new method for measuring the nonlinear phase shift. This method was specifically designed for SOA nonlinearity. In Section 4 we show our measurements of nonlinear phase shift in the 42–168-GHz range. We found that the nonlinear phase shift was straightforwardly dependent on the repetition frequency and the injection current, and this result was in line with our predictions. In Section 5 we introduce examples of results for 168-GHz regular switching (i.e., switching driven by periodic control pulses) and determine the characteristics of the nonlinear phase shift under such switching conditions. Although all the results and designs presented in Sections 3–5 are limited to those in the regular switching regime, we believe that these results provide a basis for the design of random switching in real applications such as 3R and wavelength conversion, which is still a subject of our research. Section 6 is a brief discussion, on the basis of experimental results, of switching driven by digitally coded control pulses. We also introduce an example of 168-Gbit/s pseudorandom wavelength conversion and determine the nonlinear phase shift under the conditions of the conversion. In Section 7 we draw conclusions from our results.

2. SYMMETRIC-MACH–ZEHNDER-TYPE ALL-OPTICAL SWITCHES

Three all-optical switches, each a variant of the (SMZ) switch, are depicted schematically in Fig. 1. Two of these switches are depicted, each with a different signal configuration, in Fig. 2. The types and their applications are also tabulated in Table 1. The switches in Fig. 1 are being driven (controlled) by digitally coded pulses, whereas those in Fig. 2 are being driven by divided-clock pulses. The switch in Figs. 1(a) and 2(a) has the original SMZ structure.[3] The switch in Figs. 1(b) and 2(b) is referred to as a polarization-discriminating SMZ (PD-SMZ), which is a modification of the SMZ structure.[30] The switch in Fig. 1(c), which is a simplification of the PD-SMZ structure, is referred to as a delayed-interference signal-wavelength converter (DISC).[11] The switching windows that are formed in all the switches in Figs. 1 and 2 can be nearly rectangular and have ultrafast rise and fall times. The formation of these windows is based on the SMZ switching mechanism.
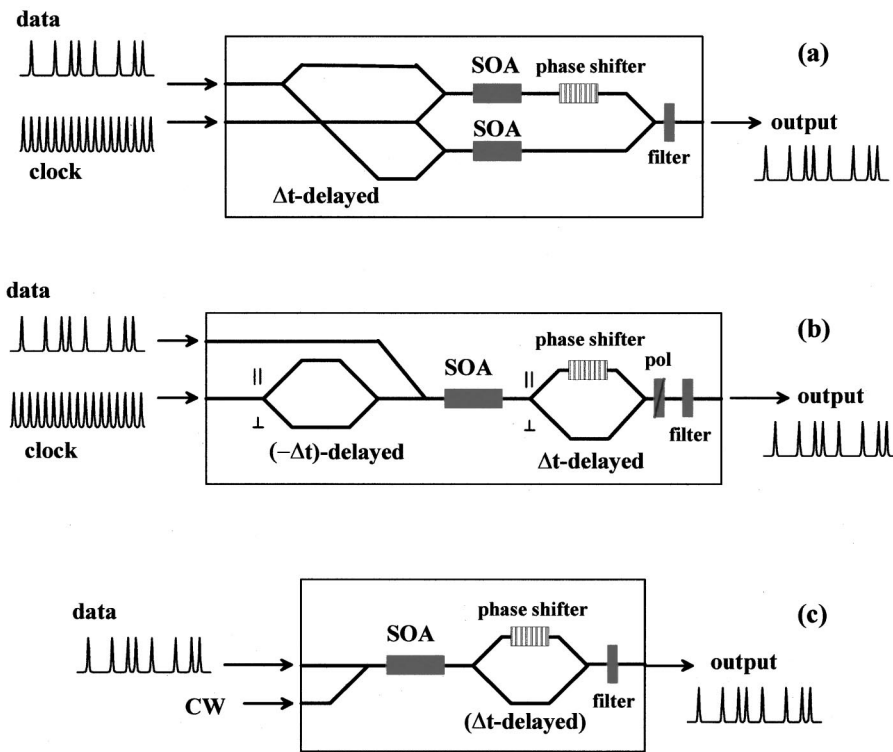
Fig. 1. SMZ-type all-optical semiconductor switches driven by digitally coded pulses: (a) a SMZ-type 3R regenerator, (b) a PD-SMZ-type 3R regenerator, (c) a DISC-type wavelength converter. pol, polarizer.
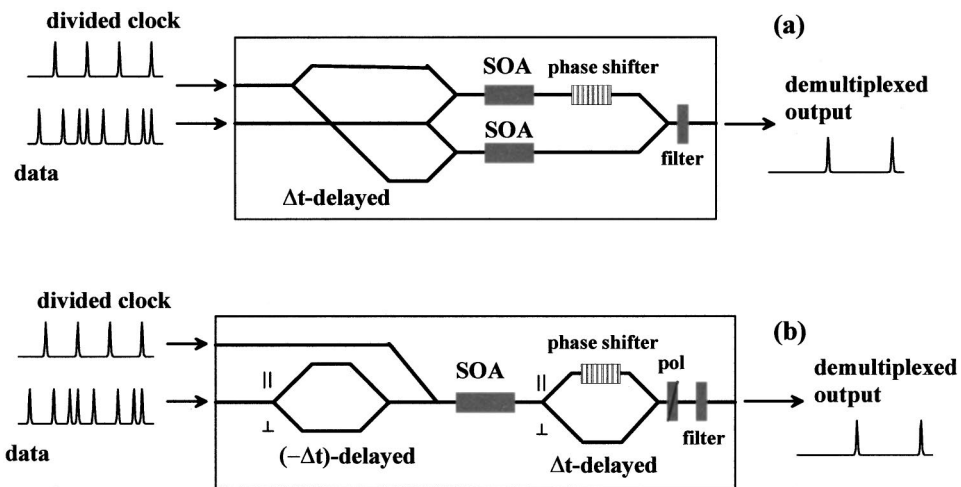
Fig. 2. SMZ-type all-optical semiconductor switches driven by regular clock pulses: (a) a SMZ-type demultiplexer, (b) a PD-SMZ-type demultiplexer. pol, polarizer.

Table 1. Three Types of SMZ Switch and Their Applications in OTDM Communications Systems

Control Scheme of the Switch	SMZ or PD-SMZ Switch[a]	DISC[b]
Data pulses control the switch (OTDM rate)	3R regeneration, asynchronous gating, logic gates (XOR, etc.)	Wavelength conversion, polarization conversion, 2R regeneration
Clock pulses control the switch (OTDM rate)	Soliton modulation	
Divided-clock pulses control the switch (electronic-time-division multiplexing rate)	Demultiplexing	

[a] Pulses are gated.
[b] cw light is gated.
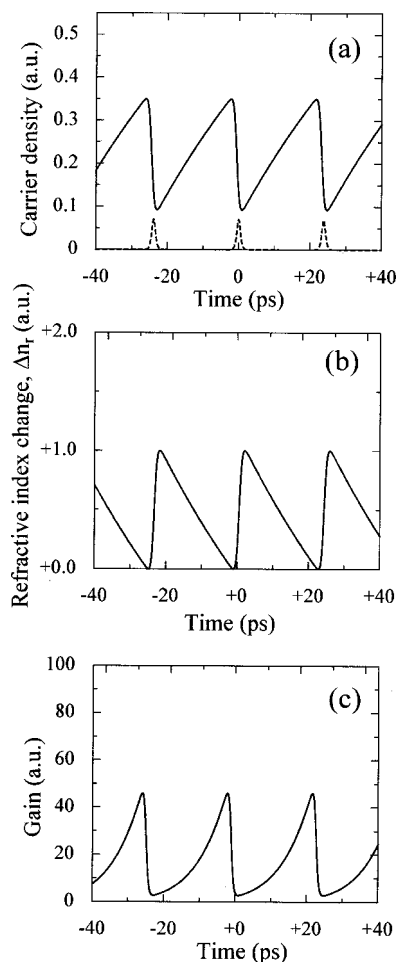
Fig. 3. Schematic view of the nonlinear phenomena inside a SOA: (a) the change in the carrier density that is induced by the optical control pulses, which causes (b) a nonlinear change in refractive index and (c) a change in the gain.   The dashed curves in (a) indicate the waveforms of the input pulses.

The configurations shown in Figs. 1(a) and 1(b) implement 3R regeneration.   The digitally coded data pulses that drive the switch arrive in an irregular (random) but nearly clock-synchronous train.   Each pulse opens a near-rectangular switching window and thus gates the precisely timed clock pulses.   Consequently, each 1 bit in the train of data pulses is replaced by a new, clean, and precisely synchronized, that is, reshaped and retimed, pulse.   The configuration in Fig. 1(c) implements wavelength conversion.

Switches in the configurations shown in Fig. 2 work as demultiplexers (or as soliton modulators), with a train of divided-frequency clock pulses (or signal-frequency clock pulses) driving the switch at regular intervals.   Note that the structure of the demultiplexer in Fig. 2(a) is exactly the same as that of the 3R regenerator in Fig. 1(a); the two devices differ only in terms of the inputs to which the respective pulses are applied.   In the same manner, only the input configuration differentiates the demultiplexer in Fig. 2(b) from the 3R regenerator in Fig. 1(b).

Figure 3 is a schematic depiction of nonlinear phenomena as they take place over time in the operation of a SOA.   In the remainder of this section, for the sake of simplicity, switching is assumed to be regular, i.e., of a

form such as that of the demultiplexer in Fig. 2 (the irregular form of switching, as required in 3R regeneration, is discussed in Section 6).   When a control pulse enters a SOA, it stimulates the recombination of carriers as a reaction to stimulated amplification.   The carrier density decreases sharply on each arrival of a pulse, and it recovers slowly until the next pulse arrives [Fig. 3(a)].   The fall time is approximately equal to the width of the control pulse.   The change in the carrier density induces change in both the refractive index [Fig. 3(b)] and the gain [Fig. 3(c)].

As a result of the nonlinear change in refractive index as shown in Fig. 3(b), the SMZ switch [see, e.g., Fig. 2(a)] forms a rectangularlike switch window for the signal pulse, as is schematically depicted in Fig. 4.   The signal pulse is split into two components at the input of the interferometer inside the SMZ switch.   The optical phase of each component is nonlinearly shifted by the nonlinear change in refractive index of the respective SOA, as is shown in Fig. 4(a).   This shifting of phase is slightly later for one of the components [dashed curve in Fig. 4(a)] than for the other [solid curve in Fig. 4(a)].   This delay time Δt
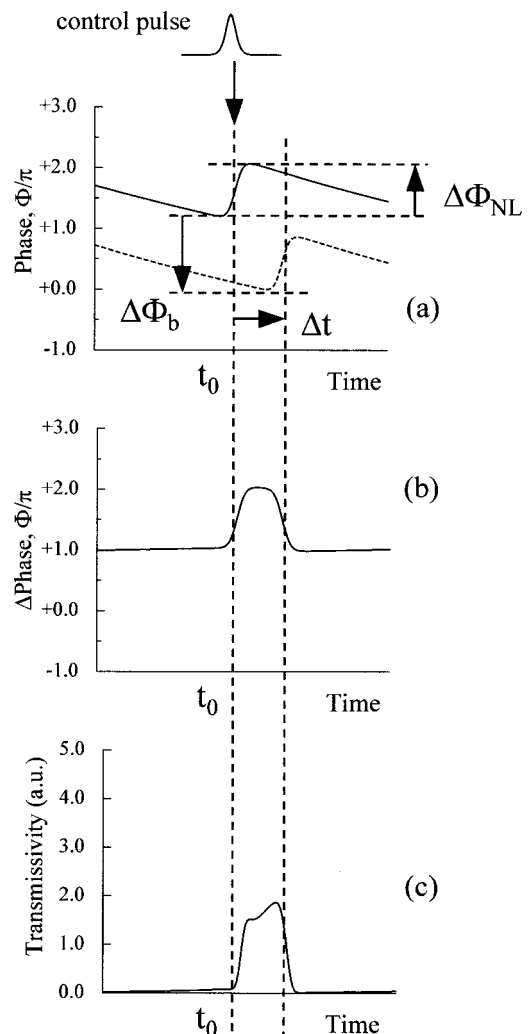
Fig. 4.   Mechanism in the SMZ-type all-optical switches: (a) Each of the two split signal components inside the interferometer obtains a nonlinear phase shift.   (b) The phase difference between the two components and (c) the switching window.
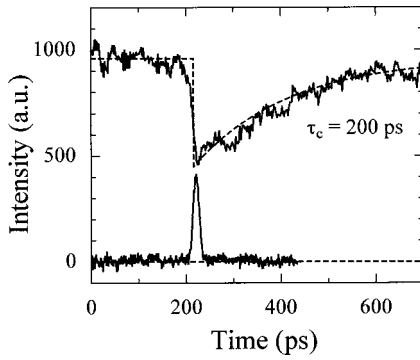
Fig. 5. Comparison of the DISC output (solid curve) and the SOA output (dashed curve) as observed with a streak camera, showing that the SMZ-type switch can form a switching window whose width is much shorter than the carrier lifetime.

is produced by the difference between the times of arrival of the control pulses at the respective SOAs [Fig. 2(a)].

The two split signal components collide and interfere with each other at the interferometer's output. The resultant complex amplitude of the signal pulse at the interference output is determined as

$$
\begin{aligned}
E_{\text{OUT}}(t) &= \tfrac{1}{2}\{\sqrt{G(t)}\exp[i\Phi(t) + \Delta\Phi_b]E_{\text{IN}}(t) \\
&\quad + [G(t - \Delta t)]^{1/2}\exp[i\Phi(t - \Delta t)]E_{\text{IN}}(t)\} \\
&= \tfrac{1}{2}\{\sqrt{G(t)}\exp[i\Phi(t) + \Delta\Phi_b] \\
&\quad + [G(t - \Delta t)]^{1/2}\exp[i\Phi(t - \Delta t)]\}E_{\text{IN}}(t) \\
&\equiv T_W(t)E_{\text{IN}}(t).
\end{aligned}
\tag{1}
$$

The phase bias $(\Delta\Phi_b)$ between the two components is adjusted such that the phase difference before t_0 and after $t_0 + \Delta t$ equals π. Consequently, the switch's transmissivity $|T_w(t)|^2$, that is, the switch window, may be approximated as a sinusoidal function of the phase difference [Fig. 4(b)] between the two components:

$$
\begin{aligned}
|T_W(t)|^2 &= |\tfrac{1}{2}\{\sqrt{G(t)}\exp[i\Phi(t) + \Delta\Phi_b] \\
&\quad + [G(t - \Delta t)]^{1/2}\exp[i\Phi(t - \Delta t)]\}|^2 \\
&= [G(t)G(t - \Delta t)]^{1/2} \\
&\quad \times \cos^2\frac{\Phi(t) - \Phi(t - \Delta t) + \Delta\Phi_b}{2} \\
&\quad + \tfrac{1}{4}\{\sqrt{G(t)} - [G(t - \Delta t)]^{1/2}\}^2.
\end{aligned}
\tag{2}
$$

Thus, in the switching window shown in Fig. 4(c), there is no carrier-relaxation-induced effect before t_0 and after $t_0 + \Delta t$. The relaxation-induced effects in the two split components have canceled each other out. The rise and fall times of the rectangularlike switching window are determined by the width of the control pulse. The width of the switching window is determined by delay time Δt.

Figure 5 shows an example of the cancellation of the relatively slow relaxation-induced effects. We used 1560-nm CW light and a streak camera to examine the formation of a switching window in a DISC by 0.7-ps 1530-nm control pulses [Fig. 1(c)]. The lower curve in

Fig. 5 shows the switch window's shape. The dashed curve in Fig. 5 follows the trace of the intensity of the cross-gain modulated continuous-wave (CW) light at the SOA output inside the DISC, which indicates a carrier relaxation time of 200 ps. Figure 5 shows that the cancellation depicted in Fig. 4 makes it possible to form a switching window that is much shorter than the carrier-relaxation time in a SMZ-type switch.

3. THEORY OF THE DYNAMICS OF THE NONLINEAR PHASE SHIFT IN A SEMICONDUCTOR OPTICAL AMPLIFIER

A. Rate Equation and Other Basic Equations for Numerical Simulation

Our approach to building a set of basic equations for use in numerically simulating the nonlinear phase shift and the all-optical switching at ultrahigh repetition frequencies is described in the following passages. First, we assume for simplicity that the changes in the refractive index and the material gain are proportional to the excess carrier density.[16] Because of this assumption, both the nonlinear phase shift and the SOA chip gain are determined by the average excess carrier density $\overline{n_c(t)}$ over the length of the SOA's active region, L. $\overline{n_c(t)}$ is defined as

$$
\overline{n_c(t)} \equiv \frac{1}{L}\int_{z=0}^{L} n_c(z, t)\,\mathrm{d}z,
\tag{3}
$$

where

$$
n_c(z, t) \equiv n(z, t) - n_{\text{tr}}.
\tag{4}
$$

Here n_c is the excess carrier density, n is the carrier density, and n_{tr} is the transparency carrier density $[G(n_{\text{tr}}) = 0]$. With the average excess carrier density $\overline{n_c(t)}$, the nonlinear phase shift [Fig. 4(a)] given to an optical component (either a pulse or a continuous wave) copropagating through the SOA is expressed as

$$
\Phi(t) = k_0 \mathrm{d}n_r/\mathrm{d}n_c[n_c{}^0 - \overline{n_c(t)}]\Gamma L,
\tag{5}
$$

where k_0 is the wave number in vacuum, n_r is the refractive index, and Γ is the optical confinement factor of these optical components within the cross section of the active layer in the SOA. The equilibrium excess carrier density, $n_c{}^0$, is defined as the excess carrier density at which the SOA does not receive any input light. The gain of the SOA chip [Fig. 3(c)] is expressed as

$$
G(t) \equiv \exp[\mathrm{d}g/\mathrm{d}n_c\overline{n_c(t)}\Gamma L].
\tag{6}
$$

Here g is the material gain. As a reference, unsaturated gain G_0 is expressed as

$$
G_0 \equiv \exp(\mathrm{d}g/\mathrm{d}n_c n_c{}^0\Gamma L).
\tag{7}
$$

Note that we no longer have to consider the distribution of carrier density along the propagation axis of the SOA because of the proportionality assumption at the be-
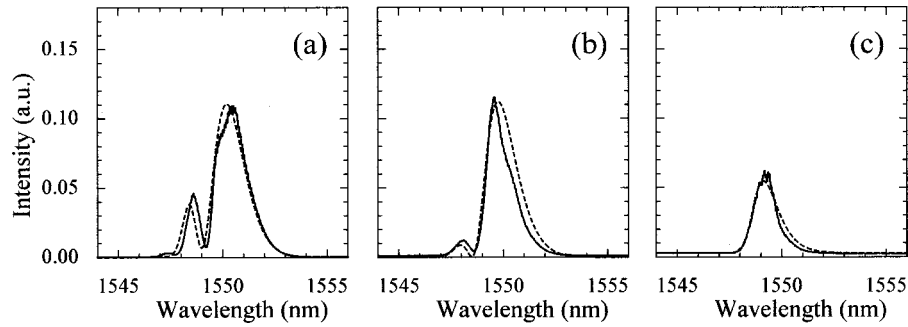
Fig. 6.   Measured (solid curves) and calculated (dashed curves) SPM spectra of the amplified 10.5-GHz 2.0-ps control pulses at the SOA output.   The input pulse energies were (a) 340, (b) 34, and (c) 3.4 fJ.

ginning of this section.   The dynamics of both the nonlinear phase shift and the chip gain as a function of time are governed by a rate equation for the average excess carrier density, which is assumed to be

$$\frac{d}{dt}\overline{n_c(t)} = \frac{I_{op}}{qV} - \frac{\overline{n_c(t)}}{\tau_c} - \frac{1}{V}\{G[\overline{n_c(t)}] - 1\}$$
$$\times \frac{|E_{control}(t)|^2 + |E_{signal}|^2}{\hbar\omega}, \qquad (8)$$

where I_{op} is the injected current, q is the elementary charge, τ_c is the carrier lifetime, and V is the volume of the current-injected active layer.   The first, the second, and the third terms on the right-hand side of Eq. (8) represent, respectively, the injection of carriers, the relaxation of carriers, and the stimulated recombination that is induced by input control pulses $[E_{control}(t)]$ and input signals $[E_{signal}(t)]$.   Note that the basic equations (5)–(8) are written in their simplest forms, on the assumption that there are no higher-order gain, higher-order changes in refractive index, or higher-order relaxation terms with respect to the carrier density.

It should be noted that the effects of carrier heating and spectral hole burning are not taken into account in basic equations (5)–(8), either.   These effects play significant roles inside SOAs when the width of the input pulses to them is shortened to less than specific values.[31–33] Nevertheless, in our simulation throughout this study we intentionally neglected these effects because the pulse widths with which we were working were slightly greater than the values given above and also because we have been interested in how well one can reproduce our experimental results numerically without taking these effects into account.   In what follows, we show that several sets of our experimental results have successfully been reproduced with this simplified model.

Finally, we take width and shape of the input pulses into account by assuming sech-type pulse shapes:

$$E_{control}(t) = \sum_m E_{control} \operatorname{sech}\!\left(\frac{t - T_m}{T_w}\right),$$
$$m = 1, 2, \ldots, \infty. \qquad (9)$$

Table 2.   Independent SOA Parameters Used for Numerical Calculation

Parameter	Description	Value
G_0	Unsaturated gain (at I_{op} = 150 mA)	28 dB
P_{sat}	Gain saturation energy (at I_{op} = 150 mA)	180 fJ
$\Delta\Phi_{max}$	Phase shift at complete depletion, $\Delta\Phi(\Delta n_c = n_c{}^0)$	$+3.0\pi$
τ_c	Carrier lifetime (at I_{op} = 200 mA)	60 ps
I_{op}	Injection current	150–250 mA

Table 3.   Derived SOA Parameters

Parameter	Description	Value
α	α parameter	$+2.9$
$n_c{}^0$	Equilibrium excess carrier density	4.8×10^{16} cm^{-3}
dg/dn_c	Differential gain	4.1×10^{-15}
dn_r/dn_c	Nonlinear change in refractive index	-1.2×10^{-19} cm^3

B.   Comparison of Measured and Calculated Semiconductor Optical Amplifier Output Spectra in Operation at 10−40 GHz

We initially verified our numerical simulation by comparing the calculated pulse gains by using Eqs. (6)–(9) and the calculated pulse gains by using a well-known form from the conventional Franz–Nodvik analysis.[34]   After this verification, we further verified our numerical simulation by comparing calculated and measured results in the following way:

Figure 6 shows measured (solid curves) and calculated (dashed curves) spectra of the amplified 2.0-ps 1550-nm control pulses at the SOA output.   The repetition frequency was 10.496 GHz (a 128th-harmonic of the repetition frequency, 82 MHz, of our synchronous streak camera).   As the input pulse energy was increased, we observed strongly self-phase-modulated (SPM) spectra. The injection current to the SOA was set to 150 mA.   A polarization-insensitive high-gain bulk-InGaAsP-active-layer SOA was used throughout the research reported

here. The SOA parameters treated in this paper are listed in Table 2. The unsaturated gain, the gain saturation energy, and the carrier lifetime were directly measured in separate experiments, in which either low-repetition rate 82-MHz pulses or a CW light were used. We only used fitting to obtain one of the parameters in Table 2 to calculate the SPM spectra in Fig. 6, that is, the phase shift at complete depletion:

$$\Delta\Phi_{\max} \equiv \Phi(n_c = n_c{}^0) - \Phi(n_c = 0)$$

$$= k_0 \mathrm{d}n_r/\mathrm{d}n_c n_c{}^0 \Gamma L. \tag{10}$$

With a $\Delta\Phi_{\max}$ value of $+3.0\pi$, our numerical simulation accurately reproduced the measured SPM spectra. Our simulation revealed that the nonlinear phase shifts involved in the respective spectra were $2.0\ \pi$ [Fig. 6(a)], 1.4π [Fig. 6(b)], and 0.75π [Fig. 6(c)].
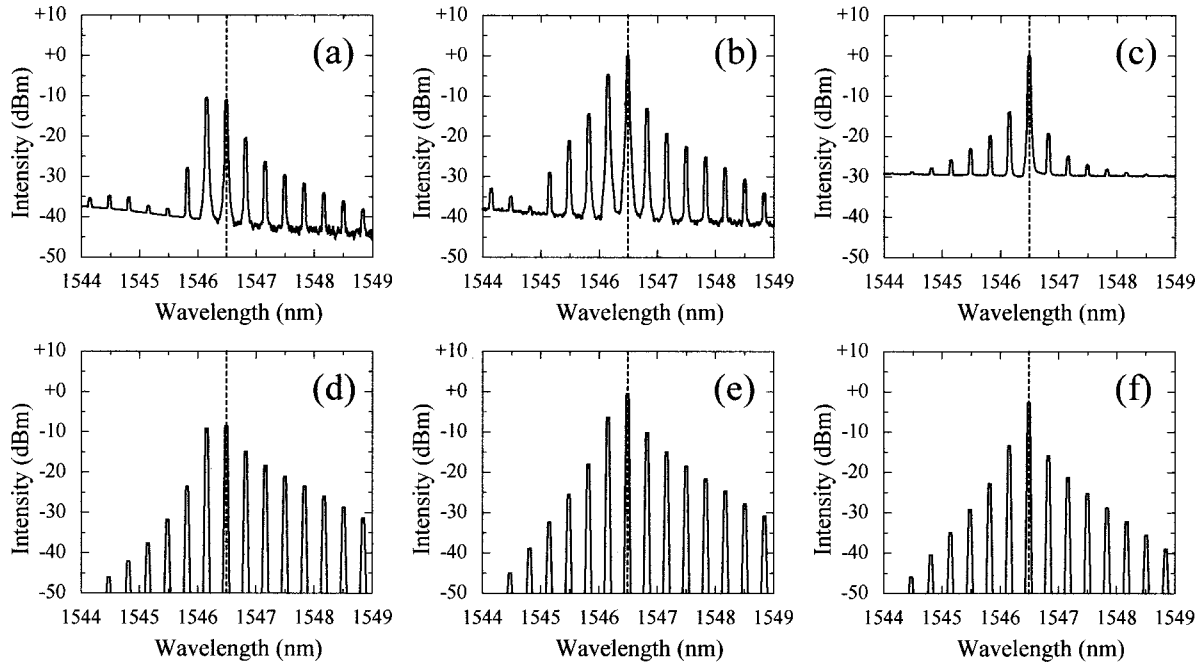
Fig. 7. Measured [(a)–(c)] and calculated [(d)–(f)] XPM spectra of the 1546.5-nm CW light at the SOA output. The input control-pulse energies were (a), (d) 100 fJ, (b), (e) 10 fJ; (c), (f) 0.3 fJ.
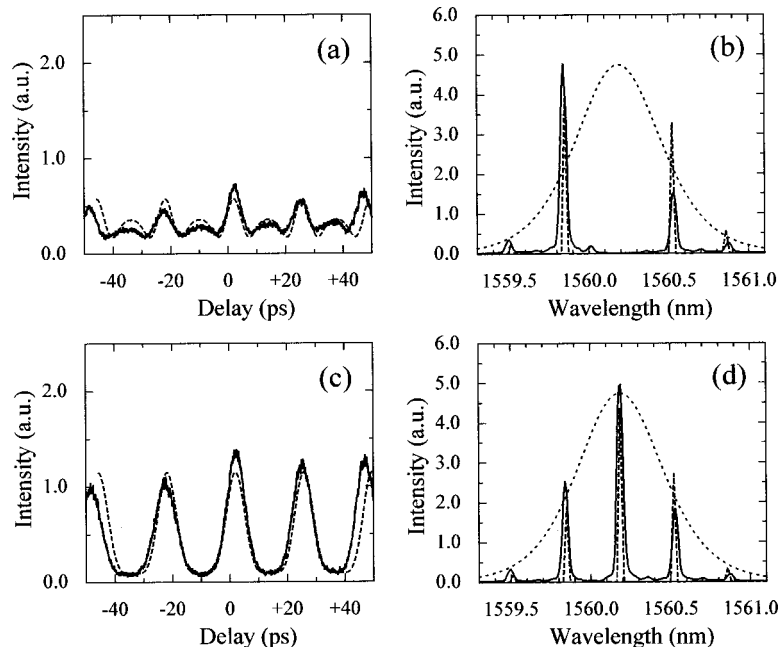
Fig. 8. Measured (solid curves) and calculated (dashed curves) autocorrelator traces (a), (c) and spectra (b), (d) of 42-GHz 7.0-ps wavelength-converted pulses at the output of the DISC: (a), (b) with the phase bias ($\Delta\Phi_b$) set to π and (c), (d) with $\Delta\Phi_b$ optimized to $1.10\ \pi$. The dotted curves in (b) and (d) are the calculated spectrum of a transform-limited 4-ps pulse, which is given as a reference.
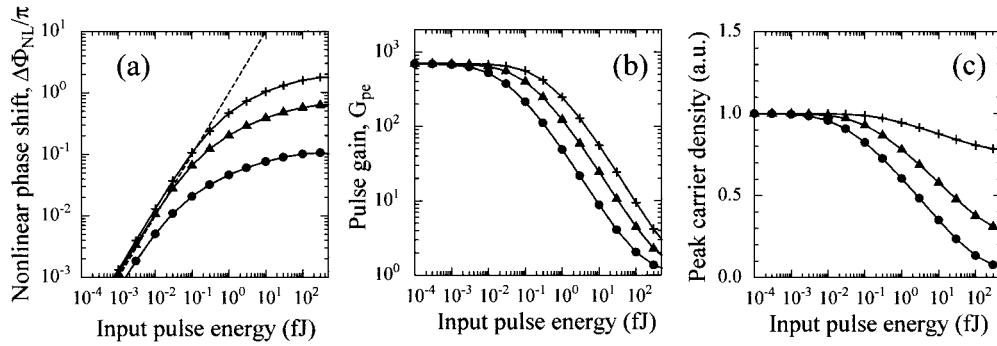
Fig. 9.   Calculated nonlinear phase shift (a), pulse gain (b), and peak carrier density (c).   The repetition frequencies of the input pulses are 10.5 (crosses), 42 (triangles), and 168 (circles) GHz.
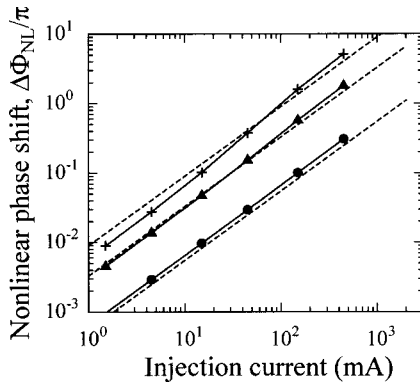
Fig. 10.   Dependences of the calculated nonlinear phase shifts of the injection current to the SOA.   The repetition frequencies are 10.5 (crosses), 42 (triangles), and 168 (circles) GHz.
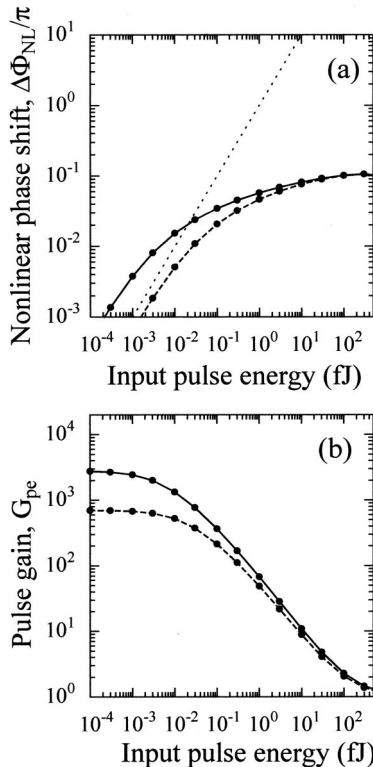
Fig. 11.   Dependences of the calculated nonlinear phase shift (a) and pulse gain (b) on the differential gain.   The unsaturated gain is assumed to be either 7000 (solid curves) or 700 (dashed curves).

The other fundamental SOA parameters were derived on the basis of the experimentally obtained parameters (Table 2) and are listed in Table 3.   The α parameter is derived from Eqs. (7) and (10) as

$$\alpha \equiv -2k_0 \frac{dn_r/dn_c}{dg/dn_c}$$

$$= -2 \frac{\Delta\Phi_{max}}{\ln G_0}. \tag{11}$$

The equilibrium excess carrier density $n_c{}^0$ was obtained from this equation:

$$n_c{}^0 = \frac{1}{V} \frac{P_{sat} \ln G_0}{\hbar\omega}. \tag{12}$$

The differential gain and the nonlinear change in refractive index were derived from Eqs. (7) and (10), respectively, with the value of $n_c{}^0$.

Here, note that the value of $n_c{}^0$ is listed in Table 3 rather than in Table 2.   We do not explicitly need the value of $n_c{}^0$ for our simulation because of assumptions of a linear change in refractive index [Eq. (5)] and linear gain [Eq. (6)] that are bases of our model.

Figure 7 shows measured and calculated spectra of the 1546.5-nm CW light at the SOA output.   Here the phase of the CW light was being cross-phase modulated by a stream of 2.0-ps 1560-nm control pulses at 42 GHz.   Each cross-phase-modulation (XPM) spectrum was split into discrete components with a spacing of 42 GHz (0.34 nm).   Note that this repetition frequency is above the SOA's cutoff frequency $[(60 \text{ ps})^{-1} = 17 \text{ GHz}]$.   Recovery of the refractive index should therefore be almost linear over time at this frequency, as is shown in Fig. 3(b).[16]   The calculated XPM spectra match the measured spectra across the range from low to high amounts of input pulse energy.   Our simulation revealed that the nonlinear phase shifts $\Delta\Phi_{NL}$ [see Fig. 4(a)] induced by the 42-GHz control pulses were 0.89π [Fig. 7(a)], 0.58π [Fig. 7(b)], and 0.37π [Fig. 7(c)].

C.   Comparison of Measured and Calculated All-Optically Switched Outputs at 40 GHz

Figure 8 shows measured and calculated autocorrelation traces and spectra of wavelength-converted pulses at the output of the DISC.[16]   In this experiment the inputs to the DISC were a 42-GHz stream of 5-ps 1548-nm pulses

and 1560.2-nm CW light; 7-ps switching windows were all-optically formed in the DISC. The CW light was gated through these windows to generate the 7-ps 1560-nm pulses at the output, which are shown in Fig. 8. When the interferometer's phase bias $\Delta\Phi_b$ was set to exactly π, however, the extinction ratio of the output pulses was very poor [Fig. 8(a)]. In this case, the output pulse's spectrum lacked its central component [Fig. 8(b)].

Here, note that the phase bias between the two interferometer components should be adjusted not to π but to an optimal value that is slightly greater than π, such that the two interference components outside the switching window interfere destructively with each other [i.e., phase difference $\Delta\Phi(t) = +1.0\pi$ at $t < t_0$ or $t > t_0 + \Delta t$ in Fig. 4(b)]. In fact, we obtained good extinction for the stream of output pulses [Fig. 8(c)] by optimizing $\Delta\Phi_b$ to 1.10π.[16] Moreover, the spectrum for these pulses has a smooth envelope [Fig. 8(d)]. All these results for the output of the all-optical switch (DISC) were reproduced surprisingly well by our simulation, which was based on Eqs. (1)–(8) and the parameters in Table 2. There was also a good match between calculated and measured transmittance of the DISC (the ratio of the peak power level of the output pulses to the power of the input cw).

D. Designing Semiconductor Optical Amplifiers for the Nonlinear Phase Shift Induced by Ultrahigh-Repetition Pulses

1. Dependencies of the Nonlinear Phase Shift on the Repetition Frequency and the Injection Current
The nonlinear phase shift imparted to the optical pulses by the SOA (Figs. 6 and 7) decreases with the repetition frequency. As a step toward the processing of signals at much higher repetition frequencies (in the 160–640-GHz range) we studied the dependencies of the nonlinear phase shift on the conditions of operation (the repetition frequency and the injection current), the parameters of the material (the nonlinear change in refractive index, the differential gain, the α parameter, and the carrier lifetime), and the structural parameters (the dimensions of the active layer and the optical confinement factor).

Figure 9(a) shows the dependence of the calculated nonlinear phase shift on the repetition frequency. The gain for the input pulses and the peak carrier density are shown for reference in Figs. 9(b) and 9(c), respectively. The peak carrier density in Fig. 9(c) represents the relative carrier density just before the arrival of each control pulse [Fig. 3(a)]. When the control pulses have little energy, the increase in the nonlinear phase shift with the pulse energy is linear. As the pulse energy is increased to increase the nonlinear phase shift, the phase shift starts to enter saturation because of gain compression [Fig. 9(b)]. Although the gain falls rapidly with increasing amounts of pulse energy, the nonlinear phase shift does not decrease but converges to a maximum value, behaving in a manner that is similar to that of the extracted pulse energy in the standard pulse-amplification regime.[34] This behavior is the result of the direct relation of nonlinear phase shift $\Delta\Phi_{NL}$ to the extracted pulse energy, $E_{out} - E_{in}$:

$$\Delta\Phi_{NL} = k_0 dn_r / dn_c \Delta n_c \Gamma L$$

$$= k_0 dn_r / dn_c \frac{1}{V} \frac{E_{out} - E_{in}}{\hbar\omega} \Gamma L. \qquad (13)$$

When the repetition frequency is 10.5 GHz, which is lower than the carrier's cutoff frequency ($\tau_c^{-1} = 16.7$ GHz), the depletion of the carrier density by one pulse has almost recovered by the time the next pulse arrives, as is indicated by the peak carrier density's being relatively close to that at the lowest level of the input pulse energy [Fig. 9(c)]. At this frequency, saturation of the nonlinear phase shift behaves in a manner similar to that of pulse amplification.

When the repetition frequency is greater than the cutoff frequency, as is the case at 42–168 GHz, the carrier density no longer recovers before the arrival of each input pulse. The values of gain fall below those at 10.5 GHz [Fig. 9(b)]. As a result, there is less nonlinear phase shift than at 10.5 GHz [Fig. 9(a)]. We believe that these are typical conditions for SOA inside an all-optical switch that is being operated at an ultrahigh repetition frequency. In our simulation of these highly saturated conditions we found that the nonlinear phase shift is inversely proportional to the repetition frequency, which is indicated to some extent by Fig. 9(a). More precisely, the maximum nonlinear phase shift induced by a train of sufficiently strong input pulses is inversely proportional to the repetition frequency as long as the repetition frequency (f_{REP}) is sufficiently greater than the carrier's cutoff frequency and sufficiently lower than the inverse of the pulse width (Δt_{pulse}), i.e.,

$$\frac{1}{\tau_c} < f_{REF} < \frac{1}{\Delta t_{pulse}}. \qquad (14)$$

Figure 10 shows the dependencies of the calculated nonlinear phase shifts on the injection current to the SOA. As indicated in the figure, we have also found that the nonlinear phase shift under a strong saturation SOA condition increases proportionally to the injection current (the dashed guidelines are for reference and indicate perfect proportionality). On the basis of Figs. 9 and 10 we conclude that, although the nonlinear phase shift at ultrahigh repetition frequency decreases with frequency, it is possible to restore the shift to π by increasing the injection current.

These theoretical proportionalities to both the repetition frequency and the injection current will be helpful in both the design and the characterization of SOAs for use in all-optical switching. The reason for these proportionalities is expressed by the rate equation, Eq. (8). When the repetition frequency is much larger than the carrier's cutoff frequency, the second term on the right-hand-side of Eq. (8) is negligible in comparison with the other two terms, that is, those that represent the carrier injection and the stimulated carrier recombination by the input pulses. These proportionalities are compared in Section 4 with their equivalents obtained by measurement.

2. Dependencies of the Nonlinear Phase Shift on the Material and Structural Parameters of the Semiconductor Optical Amplifier

Figure 11(a) indicates the dependence of the calculated nonlinear phase shift on the unsaturated gain (i.e., its dependence on the differential gain, dg/dn_c). The corresponding pulse gains are shown for reference in Fig. 11(b). The values with the unsaturated gain of 700 (dashed curves) in Figs. 11(a) and 11(b) show, for reference, the same phase shifts and pulse gains at 168 GHz as were already shown in Figs. 9(a) and 9(b), respectively. The solid curves show the phase shifts and pulse gains when an increase by a factor of 10 in the SOA's unsaturated gain is assumed. As is indicated in the figures, the nonlinear phase shift increases under the unsaturated SOA conditions but does not increase at all under the highly saturated conditions in which we are most interested here.

The smallness of the dependence on the unsaturated gain (equivalently, on the differential gain) leads us to the negative conclusion that the α parameter [Eq. (11)], which has been widely used as the standard measure of nonlinearity within SOAs, is not a good measure of the nonlinear phase shift at ultrahigh repetition frequencies. For example, the α parameter decreases when the differential gain of a SOA increases, but the saturation level of the nonlinear phase shift remains constant, according to the results shown in Fig. 11(a).

The dependencies of the nonlinear phase shift on the other material parameters, i.e., the nonlinear change in the refractive index and the carrier lifetime, are clear. The increase in the nonlinear phase shift should be proportional to the nonlinear change in the refractive index, $\Delta n_r/\Delta n_c$, according to Eq. (5). Note that carrier lifetime τ_c does not appear in Eq. (5) because it does not affect the nonlinear phase shift as long as the repetition frequency is sufficiently larger than the cutoff frequency of the carriers (τ_c^{-1}).

We also consider the dependencies of the nonlinear phase shift on the SOA's structural parameters. First, the nonlinear phase shift in Eq. (5) appears to increase with the SOA length, L. We have theoretically concluded, however, that the nonlinear phase shift is independent of L when the injection current (not the injection current density) is kept constant. This is so because the increase in the nonlinear phase shift with L is compensated for by the decrease with the carrier density that is caused by the decrease in injection current density. In contrast, the nonlinear phase shift increases with L when the injection current density (not the injection current) is kept constant.

Here we must recognize that the dependence on L mentioned above is a guideline that indicates the theoretical limit in the representation that we are using. Changing L while keeping the injection current constant will affect certain other conditions inside the SOA, such as its temperature and the quantum efficiency of carrier injection. We must take these factors into account separately from the theoretical predictions.

We used a similar approach to study the theoretical dependencies of the nonlinear phase shift on the other structural parameters. We concluded that the nonlinear

phase shift is proportional to the optical confinement factor (Γ, the ratio of the optical field confined to the active layer) and is inversely proportional to both the thickness (d_a) and the width (W) of the active layer. We summarize these dependencies as a single proportionality:

$$\Delta\Phi_{\mathrm{NL}} \propto \Gamma \frac{I_{\mathrm{op}}}{d_a W} \qquad (15)$$

or

$$\Delta\Phi_{\mathrm{NL}} \propto \frac{\Gamma}{d_a W} I_{\mathrm{op}}. \qquad (16)$$

Relation (15) is suitable for intuitive understanding and indicates that the nonlinear phase shift increases with Γ and also with the cross-sectional injection current density.

Relation (16), however, is suitable for use in optimizing the shape of the SOA's active layer in the following way: Both Γ/d_a and Γ/W have maxima, which are functions of d_a and W, respectively. This is a well-known phenomenon that is used in the design of semiconductor lasers. So we conclude from Relation (16) that there are optimum d_a and W for the active layer that maximize the value of $\Gamma/(d_a W)$. The optimum d_a is equal to the optimum W, which means that the optimum shape of the cross section of the active layer is square. Such an active layer maximizes the contribution of the injection current to the nonlinear phase shift.

All the dependencies of the nonlinear phase shift that we have discussed in this subsection are summarized in Table 4.

E. New Method for Measuring the Nonlinear Phase Shift

In general, the XPM spectrum is broadened as the nonlinear phase shift is increased (Fig. 7). The XPM spec-

Table 4. Calculated Dependences of the Nonlinear Phase Shift $\Delta\Phi_{\mathrm{NL}}$ Induced by SOAs with Input Pulses at Relatively High Repetition Frequencies f_{REP}

Property	Description	Dependency of Nonlinear Phase Shift, $\Delta\Phi_{\mathrm{NL}}$
Operating condition		
f_R	Repetition frequency	$\Delta\Phi_{\mathrm{NL}} \propto 1/f_{\mathrm{REP}}$
I_{op}	Injection current	$\Delta\Phi_{\mathrm{NL}} \propto I_{\mathrm{op}}$
Material parameter		
dn_r/dn_c	Nonlinear change in refractive index	$\Delta\Phi_{\mathrm{NL}} \propto dn_r/dn_c$
dg/dn_c	Differential gain	Independent
α	Alpha parameter	Independent
τ_c	Carrier lifetime	Independent
Structural parameter		
Γ	Optical confinement factor	$\Delta\Phi_{\mathrm{NL}} \propto \Gamma$
L	Active-layer length	Independent (for a fixed I_{op})
d_a	Active-layer thickness	$\Delta\Phi_{\mathrm{NL}} \propto 1/d_a$
W	Active-layer width	$\Delta\Phi_{\mathrm{NL}} \propto 1/W$
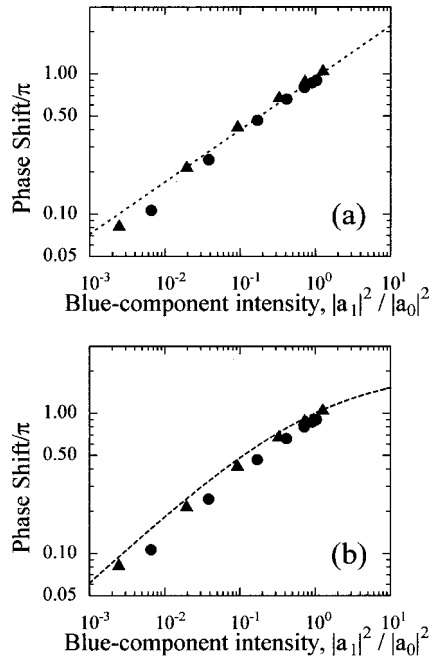
Fig. 12. Correlation of the calculated intensity ratios between components of the XPM spectrum with the calculated nonlinear phase shift induced by pulses at 42 GHz (triangles) and 168 GHz (circles). The dashed line in (a) is a line of fit to the set of data points. The dashed curve in (b) was calculated with Eq. (22) of the text.
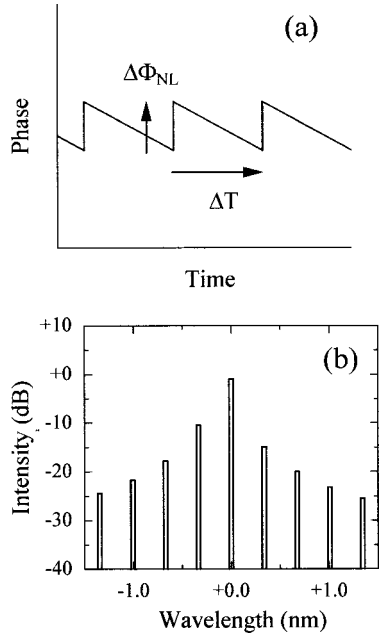
Fig. 13. Analytical derivation of the XPM spectra: (a) a simplified model of the nonlinear phase shifts, (b) 42-GHz-modulated XPM spectrum, analytically derived on the assumptions of the simplified phase-shift model and negligible gain modulation.

trum is composed of discrete components at a spacing of the repetition frequency. In carrying out the numerical simulation we noticed a useful correlation between the two phenomena. Figure 12(a) shows an example of the correlation between nonlinear phase shift $\Delta\Phi_{NL}$ and the

ratio of the first blue spectrum component to the central spectrum component, $|a_1|^2/|a_0|^2$, which were obtained with control pulses at repetition frequencies of 42 GHz (triangles) and 168 GHz (circles). We varied the amount of energy per pulse to change the nonlinear phase shift. Note that the correlation between the two values is almost independent of the repetition frequency.

In a similar way, we have numerically demonstrated that the correlation between $\Delta\Phi_{NL}$ and $|a_1|^2/|a_0|^2$ is independent not only of the repetition frequency [under the inequality condition given above, Eq. (14)] but also of the injection current, the material parameters, and the structural parameters. The correlation between $\Delta\Phi_{NL}$ and $|a_1|^2/|a_0|^2$ as calculated with various parameter values stayed close to the following function obtained by fitting:

$$\Delta\Phi_{NL} = 0.938(|a_1|^2/|a_0|^2)^{0.372}. \tag{17}$$

This function produces the dashed curve shown in Fig. 12(a). Inasmuch as the correlation between $\Delta\Phi_{NL}$ and $|a_1|^2/|a_0|^2$ is independent of all the parameters that determine the phase shift, we propose using the XPM spectrum and Eq. (17) as a way of measuring the nonlinear phase shift.

Our analytical derivation of the above correlation follows. In the derivation we assumed that (a) the pulse width is negligibly short, (b) the gain modulation is negligibly small, and (c) the carrier's cutoff frequency is sufficiently low. Under these assumptions, the modulation of the nonlinear phase by the train of control pulses is ultimately simplified to a saw-toothed shape [Fig. 13(a)] that has only two parameters, $\Delta\Phi_{NL}$ and ΔT ($\equiv 1/f_{REP}$). The nonlinear phase is expressed in terms of these two parameters in the following way:

$$E(t) \equiv \exp(-iht)$$
$$= a_0 + a_1\exp(-i\omega t) + a_2\exp(-2i\omega t)$$
$$+ a_3\exp(-3i\omega t) + \ldots$$
$$+ a_{-1}\exp(i\omega t) + a_{-2}\exp(2i\omega t) + a_3\exp(3i\omega t)$$
$$+ \ldots, \tag{18}$$

where

$$h \equiv \Delta\Phi_{NL}/\Delta T, \tag{19}$$

$$\omega \equiv 2\pi/\Delta T = 2\pi f_{REP}. \tag{20}$$

The intensity of each Fourier-transformed XPM component is derived as

$$a_n = \frac{1}{\Delta T}\int_{-\Delta T/2}^{+\Delta T/2}\exp(-iht)\exp(ni\omega t)dt$$

$$= \frac{2}{i(h-n\omega)\Delta T}\sin\frac{(h-n\omega)\Delta T}{2}$$

$$= -\frac{2i}{2n\pi-\Delta\Phi_{NL}}\sin\frac{2n\pi-\Delta\Phi_{NL}}{2}. \tag{21}$$

Thus the ratio between the XPM components is expressed as

$$\frac{|a_1|^2}{|a_0|^2} = \left(\frac{\Delta\Phi_{\mathrm{NL}}}{2\pi - \Delta\Phi_{\mathrm{NL}}}\right)^2 \sin^2\frac{2\pi - \Delta\Phi_{\mathrm{NL}}}{2} \Big/ \sin^2\frac{g\Delta\Phi_{\mathrm{NL}}}{2}. \tag{22}$$

The XPM spectrum at a $\Delta\Phi_{\mathrm{NL}}$ of 0.5π as analytically calculated by use of Eq. (21) is shown in Fig. 13(b). It provides a fairly good reproduction of the measured XPM spectrum of Fig. 7(b), for which the $\Delta\Phi_{\mathrm{NL}}$ was estimated to be 0.58π. The correlation between $\Delta\Phi_{\mathrm{NL}}$ and $|a_1|^2/|a_0|^2$ that is derived from Eq. (22) is shown by the dashed curve in Fig. 12(b). The numerically calculated data on the correlation (circles and triangles) are again surprisingly close to the analytically derived curve for the correlation. Note that

(1) The asymmetric XPM spectrum was analytically related to the saw-toothlike profile of the nonlinear phase shift,
(2) The gain modulation has very little effect on the shape of the XPM spectrum, and
(3) This method for measuring the nonlinear phase shift will be applicable to other materials that have relatively long relaxation times as well as to semiconductor materials.

4. MEASURED NONLINEAR PHASE SHIFTS AT REPETITION FREQUENCIES IN THE 40−160-GHz RANGE

We applied the new method of measurement described above to the experimental study of the nonlinear phase shift. We applied 1.5-ps pulses at repetition frequencies of 42–168 GHz and a 1547-nm CW probe light to the SOA,
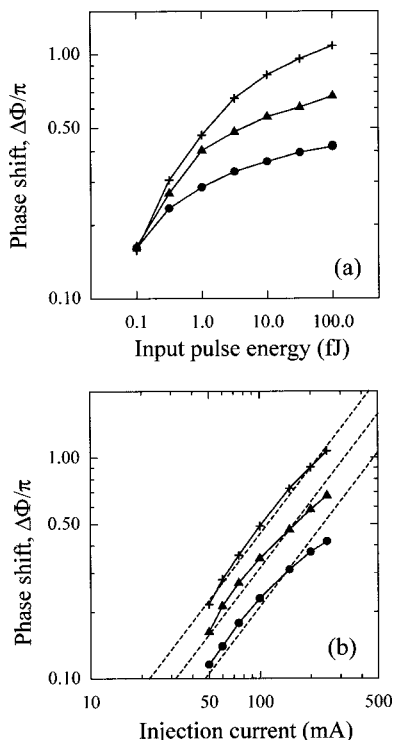
Fig. 14. Nonlinear phase shifts as measured from respective XPM spectrum ratios at the SOA's output, induced by 1.5-ps pulses at 42 (crosses), 84 (triangles), and 168 (circles) GHz.
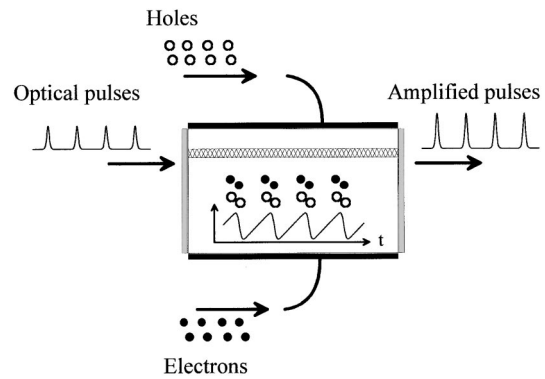
Fig. 15. Model of the nonlinear phase shift induced by a SOA by input pulses at a high repetition rate.

observed XPM spectra at wavelengths near that of the CW, and used Eq. (17) to obtain the corresponding nonlinear phase shifts, as are summarized in Fig. 14.

Figure 14(a) shows the measured nonlinear phase shifts induced by trains of pulses at 42 (crosses), 84 (triangles), and 168 (circles) GHz, as functions of the input pulse energy. The injection current to the SOA was set to 250 mA. The saturation of the nonlinear phase shift seen in Fig. 14(a) is similar to that for the calculated phase shift in Fig. 9(a). The nonlinear phase shift at saturation was approximately inversely proportional to the repetition frequency.

Figure 14(b) shows the dependence of the nonlinear phase shift on the injection current. The input pulse energy was set to 100 fJ. The dashed guidelines are for reference and indicate proportionalities. As the figure shows, the nonlinear phase shift was approximately proportional to the injection current. Thus the theoretically predicted proportional dependencies on the repetition frequency and the injection current,

$$\Delta\Phi_{\mathrm{NL}} \propto \frac{I_{\mathrm{op}}}{f_{\mathrm{REP}}}, \tag{23}$$

had been verified.

On the basis of these experimental results we have proposed an intuitive model for the nonlinear phase shift induced in a SOA by input pulses at high repetition frequencies. When a SOA receives a train of input pulses at a high repetition rate, as depicted in Fig. 15, each input pulse almost completely depletes the carrier number within the SOA. As a result, the number of carriers that are recombined on the arrival of each pulse is approximately equal to the number of carriers injected between the times of arrival for the previous pulse and for the present pulse. The nonlinear phase shift that is produced by the arrival of each pulse is proportional to the number of recombined carriers. Thus the nonlinear phase shift is inversely proportional to the repetition frequency and proportional to the injection current.

5. REGULAR SWITCHING AT 160 GHz

We performed experiments with switching at 168 GHz to demonstrate the behavior of the SMZ-type all-optical switch,[35] for which the nonlinear phase shift mentioned above is applied. Figure 16 shows the setup for our ex-

periments with switching. The high-repetition-rate train of control pulses was generated with an actively mode-locked fiber-ring laser (Pritel, Inc., Naperville, Ill.), fiber multiplexers, and Er-doped fiber amplifiers (EDFAs). The mode-locked fiber laser generates a 10.496-GHz train of 1565-nm pulses. Four stages of Mach–Zehnder-interferometer-type multiplexers precisely multiplex the repetition frequency from 10.496 to 168 GHz. The pulse width of the generated 168-GHz pulses was measured with an autocorrelator to be 2.0 ps. The maximum pulse energy coupled to the SOA was 100 fJ at 168 GHz. The 1547-nm CW light was generated with an external-cavity semiconductor laser. The CW light and the 168-GHz control pulses were combined in a 50:50 coupler for input to the SOA via a pigtailed input fiber. The coupling coefficient was 50%.

The all-optical switch used in the experiment was a DISC, i.e., the switch schematically depicted in Fig. 1(c). We used a calcite crystal, a quarter-wave plate, a Babinet–Soleil phase retarder, and polarizers to build the Mach–Zehnder interferometer (MZI) inside the DISC. The calcite crystal is birefringent to one of the two orthogonally polarized components and thus gives a delay time of 2.0 ps to the other component. An EDFA was inserted between the SOA and the Mach–Zehnder interferometer.

Figure 17 shows typical DISC outputs at 168 GHz as observed with a streak camera [Fig. 17(a)], an autocorrelator [Fig. 17(b)], and a spectrum analyzer [Fig. 17(c)]. Each input pulse had 100 fJ of energy and an average power level of 16.8 mW, and the level of input CW power was 10 μW. A large extinction ratio of the output pulses (at least 12, but measurement was limited by the streak camera's time resolution) was obtained, as shown in Fig. 17(a). The output pulse width was measured with the autocorrelator to be 2.0 ps, which was a good match with the calcite's delay time. This result indicates that the ultrafast response mechanism of the SMZ switch is still valid in switching at 168 GHz. The output spectrum's envelope approximately matched the calculated spectrum
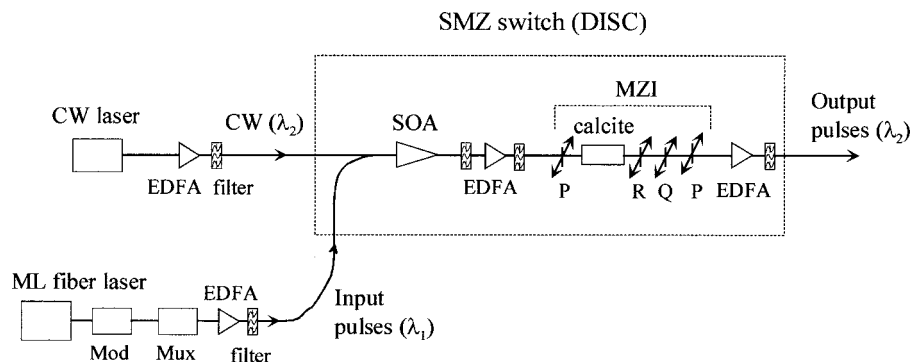
Fig. 16. Experimental setup for all-optical switching at 168 GHz. The DISC switch structure was used. Mux, multiplexer; P's polarizers; R, phase retarder; Q, quarter-wave plate; ML, mode locked; Mod, modulator.
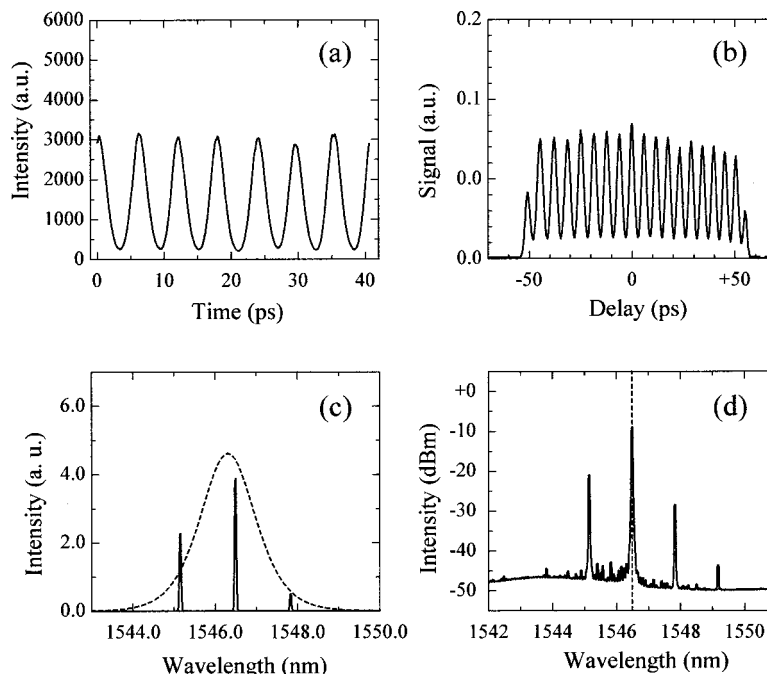
Fig. 17. Observed 168-GHz switch output waveforms: (a) streak-camera image, (b) autocorrelator trace, and (c) XPM spectrum. The nonlinear phase shift involved here was measured as 0.33π on the basis of the XPM spectrum (d) observed at the SOA output.
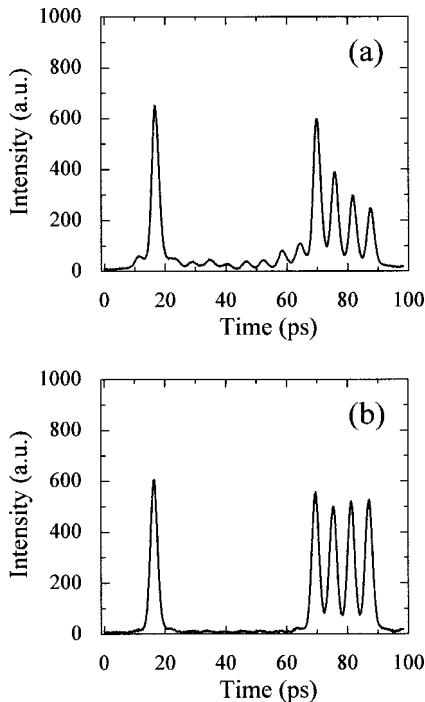
Fig. 18.   Comparison of typical output waveforms when the switch is driven at 168 GHz by digitally coded control pulses with (a) weak and (b) strong CW input.
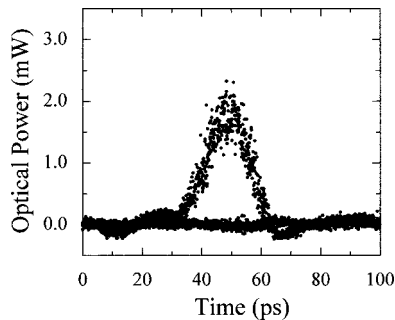
Fig. 19.   Typical eye diagram after 168-GHz random switching (wavelength conversion).   The eye diagram was measured after demultiplexing of the 168-Gbit/s wavelength-converted output to 10.5-Gbit/s signals because of the limited bandwidth of our sampling scope.

for a transform-limited 1.6-ps pulse [dashed curve in Fig. 17(c)], which suggests that the output pulse contains little chirping.[17]

We measured the nonlinear phase shift under the condition of this 168-GHz switching.   The XPM component ratio observed at the SOA's output indicated [i.e., the result in Fig. 17(d) and Eq. (17) indicated] that the nonlinear phase shift in this switching was 0.33π.

6. RANDOM SWITCHING (WAVELENGTH CONVERSION) AT 160 GHz DRIVEN BY DIGITALLY CODED SIGNAL PULSES

Using the same DISC, we demonstrated wavelength conversion [i.e., the DISC was controlled by a stream of digitally coded pulses at 168 GHz (Refs. 21, 24, and 25)] and measured the nonlinear phase shift involved under the conditions of operation.   To generate the pseudorandom

control pulses we used a 10-GHz LiNbO$_3$ modulator driven by a 12.5-GHz pulse-pattern generator (Anritsu) between the synchronized fiber-ring laser and the multiplexers of the arrangement in Fig. 16.   As has been well established, relatively strong CW input is required for operating the SMZ-type all-optical switch in such a random-switching regime.[12,36]   Figure 18 shows a comparison of typical output waveforms with weak [Fig. 18(a)] and strong [Fig. 18(b)] CW input.   Here, a 16-bit-long pattern of control pulses temporarily replaced the pseudorandom pulses, which allowed us to synchronize the waveforms with our streak camera.   The strong CW input in our experiment has effectively reduced the relaxation time of the SOA and consequently suppressed the signal-pattern-induced effects, as shown in Fig. 18(b).   This output behavior was confirmed by numerical simulation with Eqs. (1)–(8).

For the pseudorandom operation of wavelength conversion at 168 GHz, the levels of input pulse energy and CW power were optimized to 60 fJ and 24 mW, respectively. The pseudorandom pattern had a length of 2^7-1 and a mark ratio of 50%.   Figures 19 and 20 show our results for the 168-GHz wavelength conversion.   Figure 19 shows a typical output eye diagram as measured with a sampling scope.   Our sampling scope's bandwidth was 30 GHz, so the output eye was measured after the 168-GHz output was demultiplexed by a SMZ demultiplexer[10,11] to a 10.496-GHz signal.   Under these operating conditions, error-free wavelength conversion (i.e., wavelength conversion with error rates below 10^{-10}) had successfully been demonstrated.[25]   Figure 20 shows the observed pulse waveforms and spectra under the wavelength-conversion conditions.   The extinction ratio of the output pulses was 12 [Fig. 20(c)].   The output pulse width as measured from an autocorrelation trace [Fig. 20(d)] was 2.0 ps.   The output pulse width was consistent with the width of the switching window, which is in principle determined by the delay time in the calcite crystal.   This indicates that the ultrafast-response mechanism of the SMZ switches is valid for both regular and random switching at 168 GHz.

The nonlinear phase shift involved in the pseudorandom wavelength conversion was measured as $0.2-0.3\pi$. In the measurement of the nonlinear phase shift, 168-GHz continuous pulses, instead of the 168-Gbits/s pseudorandom pulses, had been applied to the DISC to generate the XPM spectrum with discrete spectral components at the SOA output, as is shown in Fig. 20(e).   As had been expected, the strong CW input decreased the nonlinear phase shift in random switching from its 0.33π value in regular switching.

Thus the performance in 168-GHz wavelength conversion was limited by the nonlinear phase shift induced by our SOA, which was fabricated according to a conventional design for use with high-gain high-saturation-power applications.   We believe that it will be possible to enhance the nonlinear phase shift by applying the new SOA design that was discussed in Subsection 3.D.

7. CONCLUSIONS

We have studied the nonlinear phase shifts induced by a semiconductor optical amplifier at driving frequencies in the range from 42 to 168 GHz.   In the study we used
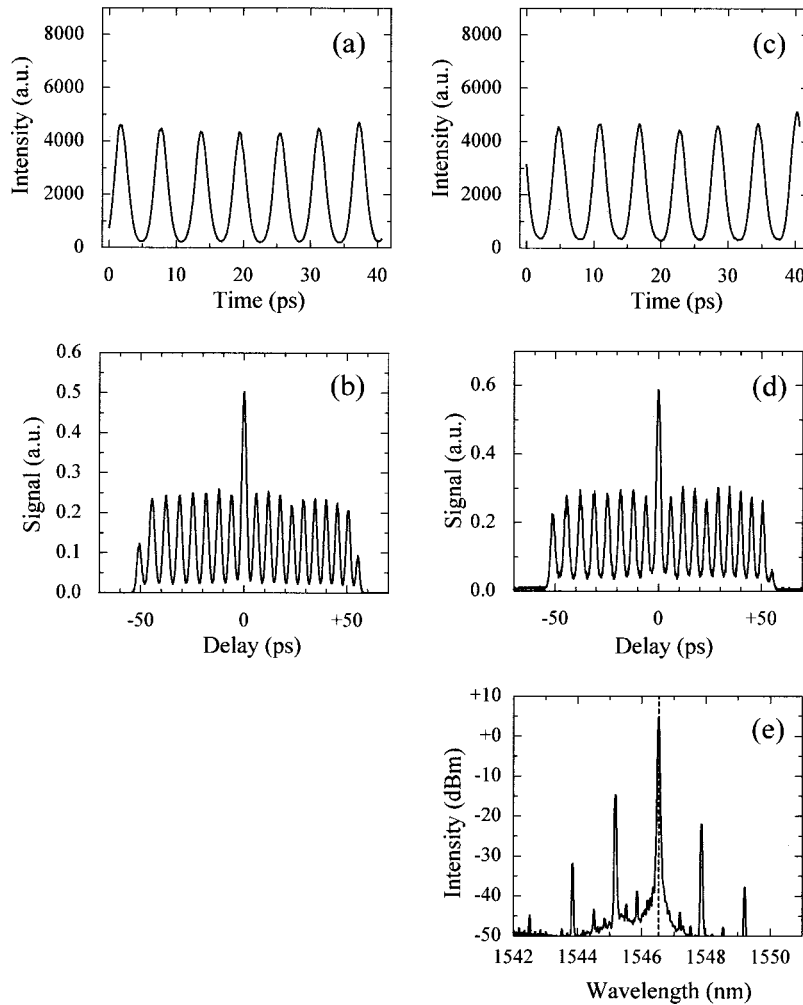
Fig. 20.   Observed pulse waveforms and spectra under the wavelength-conversion conditions: For the input pulses, (a) a streak-camera image and (b) an autocorrelation trace, and for the pulses at the DISC output, (c) a streak-camera image, (d) an autocorrelation trace, and (e) an XPM spectrum.   The nonlinear phase shift involved in this operation was measured as 0.2–0.3π on the basis of the XPM spectrum observed at the SOA output.

theory to deduce proportional dependencies of the nonlinear phase shift on the repetition frequency ($\Delta\Phi_{NL} \propto f_{REP}{}^{-1}$) and on the injection current ($\Delta\Phi_{NL} \propto I_{op}$), both of which had been believed to be more complicated because of the interplay between strong gain modulation and the nonlinear change in refractive index.   We experimentally verified both proportionalities, which are both very simple because the SOA carriers at such ultrahigh repetition frequencies are strongly depleted.   The two dependencies indicate, in a straightforward manner, that increasing the injection current is a promising way to compensate for the decrease of the nonlinear phase shift at ultrahigh repetition frequencies.

We have also theoretically determined all the other basic design factors for SOAs, i.e., the dependencies of the nonlinear phase shift on the material and structural parameters of the SOAs.   This includes the unexpected conclusion that the α parameter is not necessarily an appropriate measure.   Although most of the results and designs presented in this paper were limited to those in the regular switching regime, we believe that most of the designs (such as the dependence of the nonlinear phase shift on the injection current and the optimization of the

cross section of the SOA active layer) will be applicable to real applications in the random-switching regime such as wavelength conversion and 3R regeneration.

The results presented in this paper will be helpful in the design of SOAs as ultrafast nonlinear elements in symmetric Mach–Zehnder switches and also in the development of new nonlinear optical materials and waveguide structures for use in such ultrahigh-speed signal processors operating in the 160–640 GHz range and to push the speed limit for such devices into the region above 1 THz.

ACKNOWLEDGMENTS

Present address, Department of Electronic Engineering, University of Electro-Communications, 1-5-1 Chofugaoka, Chofu, Tokyo 182-8585, Japan; e-mail address, y.ueno@osa.org.

REFERENCES

1. N. Bloembergen, *Nonlinear Optics* (Benjamin, New York, 1965; reprinted by Addison-Wesley, Redwood, Calif., 1992).

2. A. Villeneuve, K. Al-Hemyari, J. U. Kang, C. N. Ironside, J. S. Aitchison, and G. I. Stegeman, "Demonstration of all-optical demultiplexing at 1555 nm with an AlGaAs directional coupler," Electron. Lett. **29**, 721–722 (1993).

3. K. Tajima, "All-optical switch with switch-off time unrestricted by carrier lifetime," Jpn. J. Appl. Phys., **32**, L1746–L1749 (1993).

4. S. Nakamura, K. Tajima, and Y. Sugimoto, "Experimental investigation on high-speed switching characteristics of a novel symmetric Mach–Zehnder all-optical switch," Appl. Phys. Lett. **65**, 283–285 (1994).

5. J. P. Sokoloff, P. R. Prucnal, I. Glesk, and M. Kane, "A teraherz optical asymmetric demultiplexer (TOAD)," IEEE Photon. Technol. Lett. **5**, 787–790 (1993).

6. S. Nakamura, Y. Ueno, and K. Tajima, "Ultrafast (200-fs switching, 1.5-Tb/s demultiplexing) and high-repetition (10 GHz) operations of a polarization-discriminating symmetric Mach–Zehnder all-optical switch," IEEE Photon. Technol. Lett. **10**, 1575–1577 (1998).

7. S. Nakamura, K. Tajima, and Y. Sugimoto, "Cross-correlation measurement of ultrafast switching in a symmetric Mach–Zehnder all-optical switch," Appl. Phys. Lett. **67**, 2445–2447 (1995).

8. S. Nakamura, Y. Ueno, and K. Tajima, "Femtosecond switching with semiconductor optical amplifier-based symmetric-Mach–Zehnder all-optical switch," in technical digest of the 6th International Workshop on Femtosecond Technology, Makuhari, Japan, July 13–15, 1999.

9. K. Tajima, S. Nakamura, Y. Ueno, J. Sasaki, T. Sugimoto, T. Kato, T. Shimoda, M. Itoh, H. Hatakeyama, T. Tamanuki, and T. Sasaki, "Hybrid integrated symmetric Mach–Zehnder all-optical switch with ultrafast, high extinction switching," Electron. Lett. **35**, 2030–2031 (1999).

10. S. Nakamura, Y. Ueno, K. Tajima, J. Sasaki, T. Sugimoto, T. Kato, T. Shimoda, M. Itoh, H. Hatakeyama, T. Tamanuki, and T. Sasaki, "Demultiplexing of 168-Gb/s data pulses with a hybrid-integrated symmetric Mach–Zehnder all-optical switch," IEEE Photon. Technol. Lett. **12**, 425–427 (2000).

11. K. Tajima, S. Nakamura, Y. Ueno, J. Sasaki, T. Sugimoto, T. Kato, T. Shimoda, H. Hatakeyama, T. Tamanuki, and T. Sasaki, "Ultrafast hybrid-integrated symmetric Mach–Zehnder all-optical switch and its 168 Gbps error-free demultiplexing operation," IEICE Trans. Electron. **E83-C**, 959–965 (2000).

12. B. Mikkelsen, K. S. Jepsen, M. Vaa, H. N. Poulsen, K. E. Stubkjaer, R. Hess, M. Duelk, W. Vogt, E. Gamper, E. Gini, P. A. Besse, H. Melchior, S. Bouchoule, and F. Devaux, "All-optical wavelength converter scheme for high speed RZ signal formats," Electron. Lett. **33**, 2137–2139 (1997).

13. Y. Ueno, S. Nakamura, K. Tajima, and S. Kitamura, "3.8-THz wavelength conversion of picosecond pulses using a semiconductor delayed-interference signal-wavelength converter (DISC)," IEEE Photon. Technol. Lett. **10**, 346–348 (1998).

14. L. Billes, J. C. Simon, B. Kowalski, M. Henry, G. Michaud, P. Lamouler, and F. Alard, "20 Gbit/s optical 3R regenerator using SOA based Mach–Zehnder interferometer gate," in technical digest of the 23rd European Conference on Optical Communications (ECOC '97), Edinburgh, Scotland, September 22–25, 1997.

15. D. Cotter and A. Ellis, "Asynchronous digital optical regeneration and networks," J. Lightwave Technol. **16**, 2068–2080 (1998).

16. Y. Ueno, S. Nakamura, and K. Tajima, "Record low-power all-optical semiconductor switch operation at ultrafast repetition rates above the carrier cutoff frequency," Opt. Lett. **23**, 1846–1848 (1998).

17. Y. Ueno, S. Nakamura, and K. Tajima, "Spectral phase-locking in ultrafast all-optical Mach–Zehnder-type semiconductor wavelength converters," Jpn. J. Appl. Phys. **38**, L1243–L1245 (1999).

18. St. Fisher, M. Duelk, M. Puleo, R. Girardi, E. Gamper, W. Vogt, W. Hunziker, E. Gini, and H. Melchior, "40-Gb/s OTDM to 4 × 10 Gb/s WDM conversion in a monolithic InP Mach–Zehnder interferometer module," IEEE Photon. Technol. Lett. **11**, 1262–1264 (1999).

19. C. Janz, B. Dagens, J.-Y. Emergy, M. Renaud, and B. Lavigne, "Integrated SOA-based interferometers for all-optical signal processing," in technical digest of the 26th European Conference on Optical Communications (ECOC 2000), Munich, Germany, September 3–7, 2000.

20. K. L. Hall and K. A. Rauschenbach, Opt. Lett. **23**, 1271–1273 (1998).

21. S. Nakamura, Y. Ueno, and K. Tajima, "Error-free all-optical data pulse regeneration at 84 Gbps and wavelength conversion at 168 Gbps with symmetric Mach–Zehnder all-optical switches," in technical digest of the Meeting on Optical Amplifiers and Their Applications (OAA 2000), Quebec, Canada, July 9–12, 2000.

22. Y. Ueno, S. Nakamura, and K. Tajima, "Penalty-free error-free all-optical data pulse regeneration at 84 Gb/s by using a symmetric–Mach-Zehnder-type semiconductor regenerator," IEEE Photon. Technol. Lett. **13**, 469–471 (2001).

23. A. E. Kelly, I. D. Phillips, R. J. Manning, A. D. Ellis, D. Nesset, D. G. Moodie, and R. Kashyap, "80 Gb/s all-optical regenerative wavelength conversion using semiconductor optical amplifier based interferometer," Electron. Lett. **35**, 1477–1478 (1999).

24. Y. Ueno, S. Nakamura, H. Hatakeyama, T. Tamanuki, T. Sasaki, and K. Tajima, "168-Gb/s OTDM wavelength conversion using an all-optical SMZ-type switch," in technical digest of the 26th European Conference on Optical Communications (ECOC 2000), Munich, Germany, Sept. 3–7, 2000.

25. S. Nakamura, Y. Ueno, and K. Tajima, "168-Gbit/s all-optical wavelength conversion with a symmetric Mach–Zehnder-type switch," IEEE Photon. Technol. Lett. **13**, 1091–1093 (2001).

26. T. Durhuus, B. Mikkelsen, and K. E. Stubkjaer, "All-optical wavelength conversion by semiconductor optical amplifiers," J. Lightwave Technol. **14**, 942–954 (1996).

27. C. Joergensen, S. L. Danielsen, K. E. Stubkjaer, M. Schilling, K. Daub, P. Doussiere, F. Pommerau, P. B. Hansen, H. N. Pulsen, A. Kloch, M. Vaa, B. Mikkelsen, E. Lach, G. Laube, W. Idler, and K. Wunstel, "All-optical wavelength conversion at bit rates above 10 Gb/s using semiconductor optical amplifiers," IEEE J. Sel. Top. Quantum Electron. **3**, 1168–1179 (1997).

28. B. Mikkelsen, S. L. Danielsen, C. Joergensen, R. J. S. Pedersen, H. N. Poulsen, and K. E. Stubkjaer, "All-optical noise reduction capability of interferometric wavelength converters," Electron. Lett. **32**, 566–567 (1996).

29. R. J. Manning, A. D. Ellis, A. J. Poustie, and K. J. Blow, "Semiconductor laser amplifiers for ultrafast all-optical signal processing," J. Opt. Soc. Am. B **14**, 3204–3216 (1997).

30. K. Tajima, S. Nakamura, and Y. Sugimoto, "Ultrafast polarization-discriminating Mach–Zehnder all-optical switch," Appl. Phys. Lett. **67**, 3709–3711 (1995).

31. C. T. Hultgren and E. P. Ippen, "Ultrafast refractive index dynamics in AlGaAs diode laser amplifiers," Appl. Phys. Lett. **59**, 635–637 (1991).

32. Y. Ueno, S. Nakamura, K. Tajima, and S. Ishikawa, "Effect of spectral hole burning on symmetric Mach–Zehnder all-optical switch," in technical digest of the 4th International Workshop on Femtosecond Technology, Tsukuba, Japan, February 13–14, 1997.

33. S. Nakamura, Y. Ueno, and K. Tajima, "Femtosecond switching with semiconductor-optical-amplifier-based sym-

metric Mach–Zehnder-type all-optical switch," Appl. Phys. Lett. **78**, 3929–3931 (2001).

34. A. E. Siegman, "Pulse amplification with homogeneous gain saturation," in *Lasers*, A. Kelly, ed. (University Science, Orlando, Fla., 1986), Chap. 10.

35. Y. Ueno, S. Nakamura, and K. Tajima, "Ultrafast 168 GHz 1.5 ps 1 fJ symmetric-Mach–Zehnder-type all-optical semiconductor switch," Jpn. J. Appl. Phys. **39**, L806–L808 (2000).

36. R. Manning and D. A. O. Davies, "Three-wavelength device for all-optical signal processing," Opt. Lett. **19**, 889–891 (1994).